Automotive Experiences
Vol. 7 No. 3 (2024) pp. 406-417
p-ISSN: 2615-6202 e-ISSN: 2615-6636

Research Paper

Development of an Automatic Coupler for Railway Vehicles: A Topology Optimization Approach with Numerical and Experimental Validation

Jean Mario Valentino[1,2], **Agus Sigit Pramono**[3], **Achmad Syaifudin**[3], **Lukman Shalahuddin**[2], **Mustasyar Perkasa**[4], **Katsuhiko Sasaki**[5]

[1]Graduate Program of Mechanical Engineering, Institut Teknologi Sepuluh Nopember, Surabaya, 60111, Indonesia
[2]Research Center for Transportation Technology, National Research and Innovation Agency, Jakarta, 10340, Indonesia
[3]Department of Mechanical Engineering, Institut Teknologi Sepuluh Nopember, Surabaya, 60111, Indonesia
[4]Structural Strength Technology Laboratory, National Research and Innovation Agency, Jakarta, 10340, Indonesia
[5]Faculty of Engineering, Hokkaido University, Sapporo, Hokkaido, 060-8628, Japan

pramono@its.ac.id

https://doi.org/10.31603/ae.11494

Published by Automotive Laboratory of Universitas Muhammadiyah Magelang

Article Info
Submitted:
04/06/2024
Revised:
15/11/2024
Accepted:
16/11/2024
Online first:
13/12/2024

Abstract

Topology optimization has demonstrated its effectiveness in generating lightweight and structurally efficient designs. This study focuses on refining the geometry of an automatic coupler body for trains using solid isotropic material with penalization and a level set method. These optimization methods are applied to the numerical model of the automatic coupler, and their results are compared to select the optimal design. The tensile strength of the automatic coupler is examined through numerical simulations and validated by experimental tensile tests conducted on a 1:1 scale prototype. The optimization outcomes reveal a remarkable 46.41% reduction in the mass of the automatic coupler body compared to the initial model. An evaluation of the tensile strength of the prototype demonstrates the ability of the automatic coupler to withstand the primary load without undergoing plastic deformation. Furthermore, a strong correlation is observed between the numerical and experimental results. This research contributes to advancing the design of next-generation automatic couplers, emphasizing the crucial aspects of lightweight design and structural performance.

Keywords: Topology optimization; Automatic coupler; Lightweight design; Tensile test; Verification and validation

1. Introduction

The lightweight design of railway vehicles is a primary focus for reducing energy consumption and operational costs. Overly heavy trains at high speeds can lead to energy waste during acceleration and increased loads on the braking system during deceleration [1]. Weight savings can be achieved through the use of lightweight components, the employment of lightweight materials, and the integration of new technologies into the train structure, resulting in reduced power consumption, lower inertia, decreased track wear, and the ability to carry larger loads [2]–[4]. Mass reduction can be considered in terms of both materials and design. A design approach, such as topology optimization, is essential because it allows for the identification of designs that minimize material usage by optimizing material distribution within the structure [5], [6].

Topology optimization (TO) is a design approach that used computer-aided engineering (CAE) to generate a diverse range of design alternatives while adhering to specific rules, constraints, and criteria [7]. Within the realm of generative design, TO has emerged as a pivotal tool for achieving structurally optimal material

shapes and distributions [8], [9]. This methodology facilitates the creation of design alternatives that not only enhance structural efficiency but also consider optimal material distribution, thereby eliminating unnecessary materials and reducing the overall weight of the structure while maintaining the desired performance [10]. TO involves several essential stages. Initially, design variables are determined to outline the aspects of the design that can be modified. Subsequently, constraints are established to delineate the components of the design that remain unalterable. Then, the optimization objectives are defined, and manufacturing constraints are identified to ensure that the optimization results can be seamlessly incorporated into the manufacturing process [11]. TO provides design forms with material distribution based on optimal force transfer paths within the design domain, resulting in designs with reduced mass [12].

TO has found application in creating design solutions, particularly in the realm of rail vehicles that demand lightweight designs, such as light rail and high-speed trains. Research endeavours have explored material reduction in components such as bogies and bolsters [13], optimization of the transmission structure in light vehicles [14], structural optimization of braking components [15] and crashworthiness components in train carbodies [16], [17]. The lightweight design focus extends to coupler designs in rail vehicles, where couplers play a critical role in connecting trainsets. While attempts to reduce the mass of automatic couplers using TO have been made on hooked plate components [18], these studies have yet to optimize the component with the largest mass—the body of the automatic coupler.

This study aims to obtain a geometrically lightweight shape for an automatic coupler body using the TO method. The designed automatic coupler body is subsequently subjected to verification and validation processes, with static simulation using finite element software for verification and tensile strength testing on prototypes for validation. The ratio of stress and strain at critical points of the automatic coupler body is also evaluated. The distinctive aspect of this research lies in the comparison of two TO methods to derive optimal geometric shapes. As integral steps in the product development process, verification and validation play a crucial role in ensuring that the design meets established quality and performance standards [19]. This research aims to contribute to enhancing the performance of next-generation automatic coupler models.

2. Methods

The method employed in this study integrates numerical design stages with subsequent experimental validation. The overall research process is outlined in **Figure 1**, illustrating the sequential steps undertaken in this investigation. The following subsections provide a detailed description of each stage, including the numerical design process and the subsequent experimental validation steps.

2.1. 3D Numeric Model

A 3D computer-aided design (CAD) model of the automatic coupler head was created using SolidWorks software, as depicted in **Figure 2**. The primary dimensions of the automatic coupler are 400 mm in length, 450 mm in width, and 150 mm in height. The key components of the automatic coupler include the upper body, lower body, hooked plate, and coupling link [20]. The total mass of the initial model is 40.74 kg, with the hooked plate weighing 6.18 kg, the coupling link

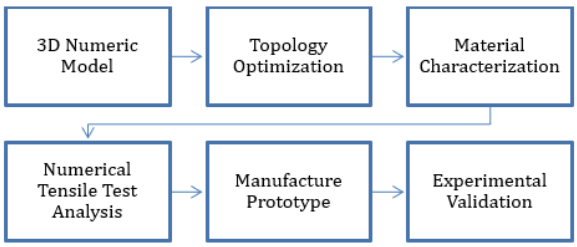

Figure 1. Proposed method

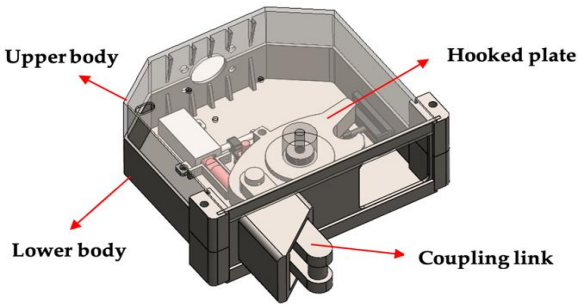

Figure 2. Initial model automatic coupler

3.19 kg, and the upper and lower bodies 31.07 kg. For TO, the initial step involves defining the maximum limits of the design space, as illustrated in **Figure 3**. Subsequently, TO is conducted to determine the optimal topographic shape for efficiently transferring forces from the coupler's end to the hooked plate.

2.2. *Topology Optimization*

There are several topology optimization (TO) models, including solid isotropic material with penalization (SIMP), the level set method (LSM), evolutionary structural optimization (ESO), and bidirectional ESO (BESO) [21], [22]. In the realm of CAE software, ANSYS employs SIMP and LSM because these two optimization models are considered the most mature [23]. SIMP optimizes material distribution by determining the density of each element in the model and utilizing quality control to manage material distribution [24]. On the other hand, the LSM optimizes the material distribution by establishing boundary lines between the filled and empty parts in the model [25].

The fundamental concept of SIMP [24], [26] involves the discretization of the design domain (Ω) using a finite element mesh. This process assigns a density value ρ_i to each element within the range of 0 to 1, where 0 signifies an empty element, and 1 represents an element filled with material. The relationship between the Young's modulus (E) and the density of an element ($E\rho e$) is expressed by Eq. (1).

$$E(\rho e) = \rho_e^p E_0 \tag{1}$$

In this equation, E_0 denotes the Young's modulus of the specified isotropic material, and the term ρe represents the relative density factor. The equation illustrates how Young's modulus can be continuously adjusted based on the material distribution represented by relative density factors. The penalty factor ρ is introduced to diminish the contribution of elements with intermediate density to the total stiffness. It guides the optimization solution toward either solid elements ($\rho e = 1$) or empty elements ($\rho e = \rho_{min}$). A decrease in the modulus of material elasticity leads to a decrease in the rigidity of the element. Following the SIMP approach, the modulation of the global rigidity is described by Eq. (2).

$$K_{SIMP\,(\rho)} = \sum_{e=1}^{N} [\rho_{min} + (1 - \rho_{min})\rho_e^p] K_e \tag{2}$$

where, K_e represents the element stiffness matrix, ρ_{min} is the minimum relative density, ρe is the element relative density, ρ is the penalty factor, and N is the number of elements in the design domain.

In the level set method (LSM), material geometry and distribution information are represented through level set functions. The level set function describes the boundary surface between a vacuum and the material, with its value indicating the distance of a point to that surface. LSM offers a notable advantage in handling topological changes without the necessity for complex remeshing [27]. Conceptually, LSM can be likened to advanced shape optimization, functioning similarly to conventional shape optimization, where the design is altered by moving boundaries while simultaneously undergoing topological changes. The design boundary is implicitly represented as the isosurface (level set zero) of the function $\emptyset(x)$, defined in the finite element mesh, as shown in Eq. (3).

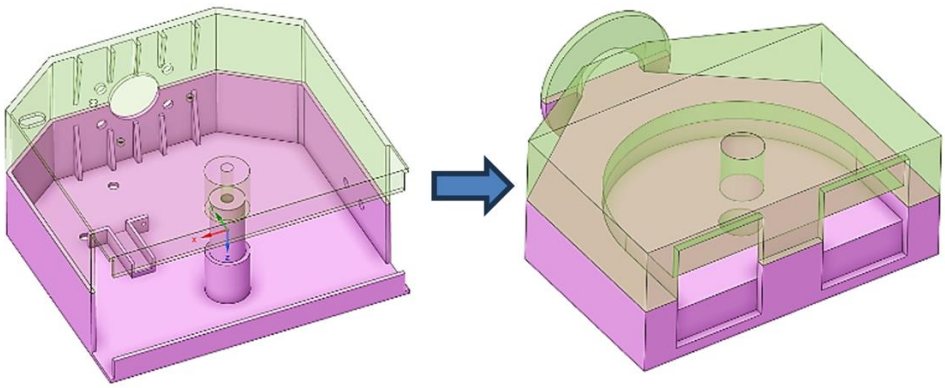

Figure 3. Formation of the design space from the initial model

$$\begin{aligned} \emptyset(x) > 0 : x \in \Omega/\partial\Omega \\ \emptyset(x) = 0 : x \in \partial\Omega \\ \emptyset(x) < 0 : x \in \mathrm{D}/\Omega \end{aligned} \quad (3)$$

where, D is the design domain; Ω is the material region, $\partial\Omega$ is the boundary and D/Ω is the region without material. The dynamic motion of the boundary is governed by the set-level equation, as expressed in Eq. (4).

$$\frac{\partial \emptyset}{\partial t} = v_n |\nabla \emptyset| \quad (4)$$

In this equation, v_n represents the normal speed and $|\nabla\emptyset|$ is the gradient of the level set function. The fundamental idea behind level set equations is to correlate the evolution of boundaries with the evolution of level set functions $\emptyset(x)$.

The objective of this phase is to minimize the design space while achieving an optimal material distribution. The variable design in this context is the density of the element. Constraints are applied within the force area, specifically at the shaft hole, hooked plate, and fixture on the flange connected to the shank coupler. Two optimization methods, namely SIMP and LSM, are employed for coupler body formation.

The mesh within the design space consists of tetrahedrons with a homogeneous element size of 10 mm, resulting in 211,766 nodes and 145,044 elements. Fixed support is applied to the flange section, and a force of 296.65 kN is applied at the shaft hooked plate hole. The optimization region encompasses the entire 3D body, while the boundary conditions determine the exclusion region. Both SIMP and LSM are chosen as optimization techniques, utilizing identical parameter settings. In the objective section, the response type is specified to minimize compliance based on static structural analysis. In the response constraint section, the mass is constrained to be at least 10%, with a maximum of 500 iterations, a minimum normalized density of 0.001, and a penalty factor (stiffness) of 3.

2.3. *Material Characterization*

The material chosen for the prototype is low-carbon steel, and its composition has been previously analysed using an optical emission spectrometer (OES). Material characterization involves conducting tensile tests to determine both the yield strength and ultimate tensile strength of the material. These properties serve as essential input parameters in the ANSYS data engineering process. The tensile test specimens adhered to the ASTM E8 standard [28], as illustrated in **Figure 4**, and the dimensions are detailed in **Table 1** [29].

Tensile testing was performed using a Shimadzu universal testing machine with a capacity of 250 kN, and the obtained stress-strain curve is presented in **Figure 5a**. The yield strength, determined at an offset stress of 0.2%, was 241 MPa, while the ultimate stress reached 360 MPa. The mechanical properties that have been input into the ANSYS engineering data are displayed in **Table 2**.

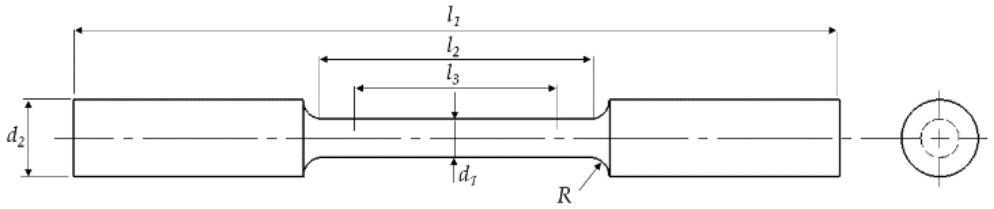

Figure 4. Tensile test specimen

Table 1. Dimensions of specimens

Symbol	Description	Dimension (mm)
L1	Length overall	200
L2	Length of the narrow section	56
L3	Gage length	50
D1	Diameter of the narrow section	12.5
D2	Diameter of the grip section	20
R	Radius of fillet	10

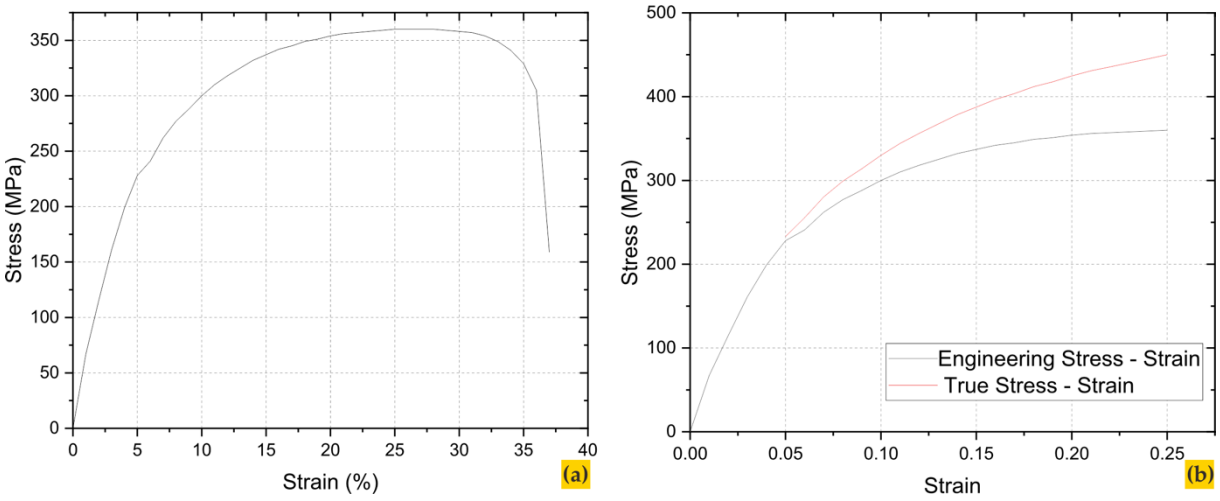

Figure 5. (a) Engineering stress-strain curve; (b) True stress-strain curve

Table 2. Mechanical properties

Material properties	Value
Young modulus (E)	200
Poisson's ratio (v)	0.3
Density (kg/m^3)	7850
Tensile Yield strength (MPa)	241
Tensile Ultimate strength (MPa)	360

For accurate finite element modelling, the precise input of material properties for each elastic and plastic condition is essential. In plastic regions, particularly in strain-hardening areas, engineering stress-strain data are converted into true stress–strain data. The true stress–strain becomes crucial when the material undergoes substantial plastic deformation under loading. Unlike engineering stress, which assumes a fixed cross-sectional area, true stress takes into account the actual change in the material's cross-sectional area [30], [31]. The conversion equations are as follows Eq. (5) and Eq. (6).

$$\sigma_{true} = \sigma_{engineering}\,(1 + \varepsilon_{engineering}) \quad (5)$$

$$\varepsilon_{true} = \ln\,(1 + \varepsilon_{engineering}) \quad (6)$$

At the design level, engineering stress–strain is commonly used, as design applications typically do not tolerate plastic deformation. However, in this study, prototype tensile testing was carried out until failure. Therefore, structural analysis and numerical simulations employed true stress and true strain to more accurately model material behaviour. The true stress-strain curve from the yield point to the ultimate point is represented using Eq. (5) and Eq. (6), as depicted in **Figure 5b**.

2.4. *Numerical Tensile Test Analysis*

To verify the design, tensile tests were simulated using ANSYS static structural modules to assess the tensile strength by analysing the stress distribution and identifying critical points for potential plastic deformation. The analysis covered the topology-optimized body and the entire assembly. Meshing was conducted with identical settings to those used in the topology optimization analysis. A fixed joint was applied to the rear cover, and a uniaxial force of 296.65 kN was applied to the front cover, following the coupler force calculation method [18]. This uniaxial force facilitates the prediction of stress using principal stress analysis. The material data input utilized multilinear isotropic hardening, requiring separate inputs for plastic and elastic material properties. The elastic data included Young's modulus and Poisson's ratio, while the plastic data consisted of coordinate data on the true stress–strain curve, starting from 0 strains to the yield strength. Solver controls were configured to activate large deflection and substep options, mitigating the possibility of plastic deformation during the analysis.

2.5. *Prototype Manufacture*

Designing using TO introduces complexities in the generated design, making traditional manufacturing challenging. Typically, implementing TO results involves additive manufacturing, specifically 3D printing, due to its ability to realize designs with intricate geometries [32], [33]. However, for steel components with substantial dimensions, the sand casting method is more practical [34]. The prototype is

manufactured at a full-scale ratio of 1:1 to ensure a precise representation. Full-scale prototypes serve to identify potential failures or weaknesses in the design, providing valuable insights for the evaluation of future production processes. Before experimental testing, the prototype underwent a thorough check using magnetic particle inspection (MPI) to guarantee the absence of porosity or cracks in critical areas. This MPI inspection is a commonly employed practice in the railway industry during overhauling and assembly processes [35], [36].

2.6. *Experimental Validation*

The objective of the experimental validation is to determine the tensile strength of the automatic coupler prototype while corroborating the numerical findings. The loading type applied is uniaxial tension, requiring the use of a single-direction strain gauge [37], [38]. The strain gauge employed is a FLAB 6-11 from Tokyo Measuring Instruments Lab, which is aligned with the normal stress direction of the simulation results. Tensile testing was conducted on an RHZ horizontal tensile testing machine with a maximum capacity of 4000 kN. During the tensile test, the prototype is subjected to a continuously increasing tensile load until it reaches failure. The testing equipment includes the RHZ horizontal tensile testing machine, a Kelsey load controller to regulate the tensile machine, step sensors, a displacement transducer for measuring machine displacement, and data loggers for recording force and strain. The collected strain and load data will be compared with the numerical simulation results to validate the accuracy of the simulations.

3. Results and Discussion

3.1. *Topology Optimization Comparison*

The shape of the automatic coupler body is predicted using two predefined TO methods, both utilizing 10% of the design space volume and 10% of the design space mass. The optimization results obtained by employing SIMP are presented in **Figure 6**, which depicts the material distribution within the design domain. Notably, the SIMP method converges in fewer iterations (31 iterations) than the LSM (53 iterations), resulting in a faster solution and computational process. However, the SIMP method produces a somewhat rough geometry, necessitating further interpretation by the designer. At convergence, the mass and volume density based on the SIMP are 2.46 kg and 0.291e2 mm greater, respectively, than those based on the LSM.

The optimization results obtained using the LSM are illustrated in **Figure 7**, showing advantages related to the boundary form during the optimization process. Boundary parts, such as shaft holes, exhibit a neat structure, and the resulting contour is smoother and more regular. Although the LSM method offers a more readily interpretable form for designers, it requires more iterations to achieve convergence, leading to higher computational costs.

The final design of the auto coupler body was determined through a combination of SIMP and LSM methods, with minor design modifications, including a symmetrical square arm cross-sectional shape and elimination of the centre hole to simplify the manufacturing process. Furthermore, an extension was added into the front shaft hole to attach the front cover. The optimized body design and the complete automatic

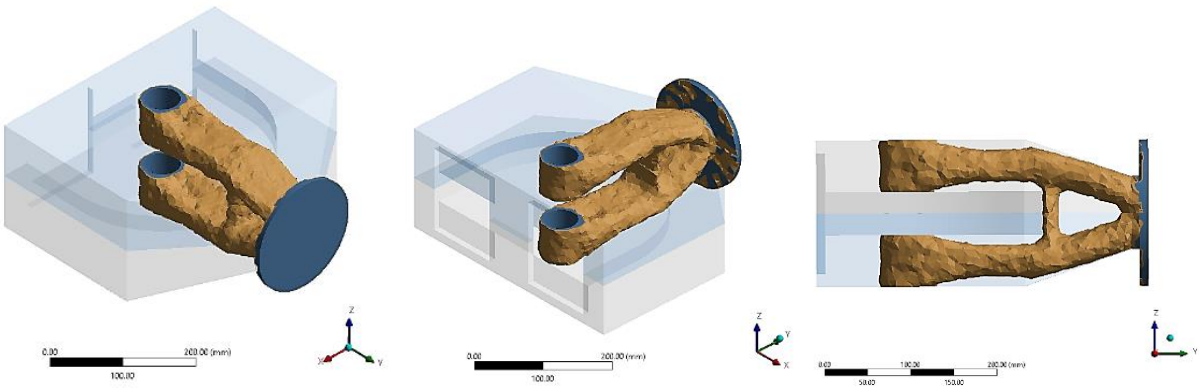

Figure 6. Three views of the SIMP method results

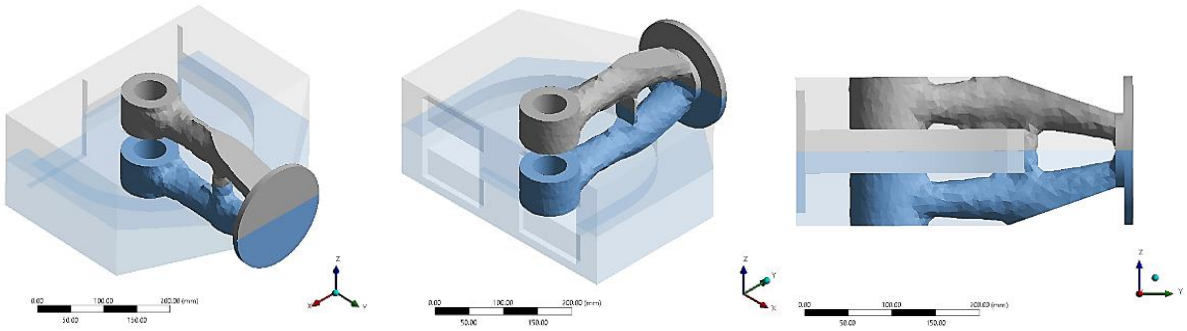

Figure 7. Three views of the LSM results

coupler assembly are shown in **Figure 8**. This modified design requires verification through tensile stress analysis before manufacturing. **Table 3** provides a comparison between the initial design, design space, SIMP, LSM, and final design. The prototype of the automatic coupler body, along with the entire assembly from the sand casting results, is presented in **Figure 9a** and **Figure 9b**.

The results of this topological optimization align with previous research conducted by Valentino [18], in which a mass reduction of 24% was achieved for the hooked plate component of the automatic coupler using the SIMP method, resulting in an overall reduction of approximately 4% for the coupler as a whole.

3.2. *Numerical Tensile Test Results*

The maximum von Mises stress on the body is observed at the shaft holes, with a factor of safety of 1.35 when compared to the yield stress of the material, as illustrated in **Figure 10a**. Simultaneously, the maximum von Mises stress in the assembly is observed in the coupling link,

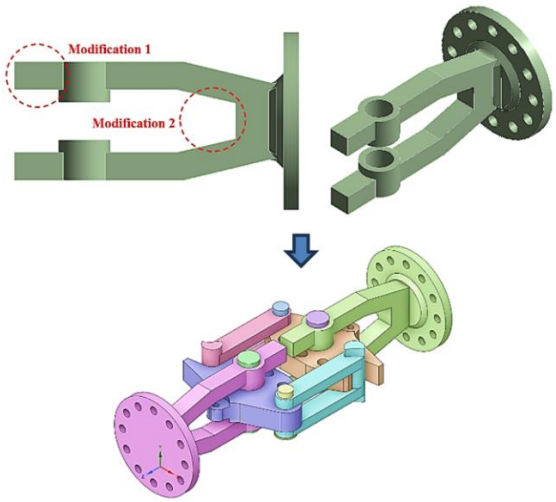

Figure 8. Optimized body design, and their assembly

Table 3. Comparison results

Experiment	Initial body design	Design Space	SIMP method	Level set method	Optimized body design
Mass (kg)	31.07	132.14	15.507	13.045	16.65
Volume (mm^3)	2.246e6	1.683e7	1.974e6	1.661e6	2.121e6
Iteration to convergence	-	-	17	23	-

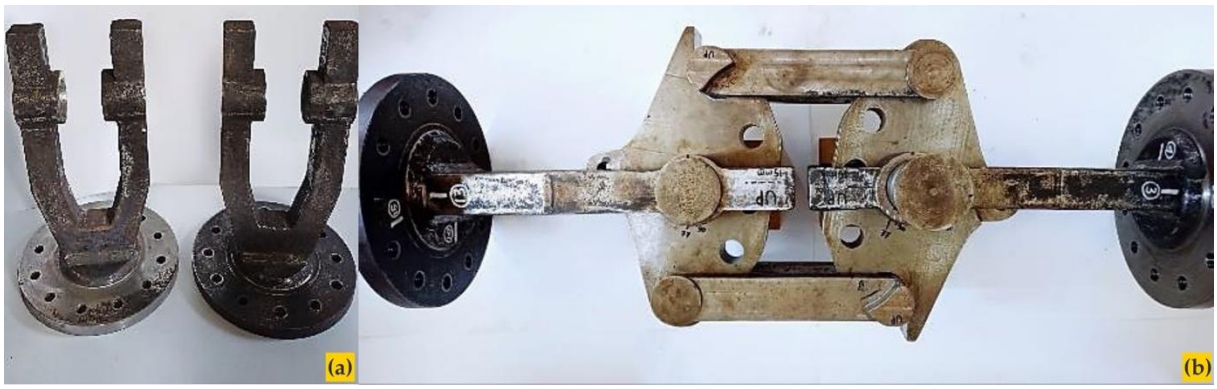

Figure 9. (a) Optimized body design; (b) Assembly automatic coupler

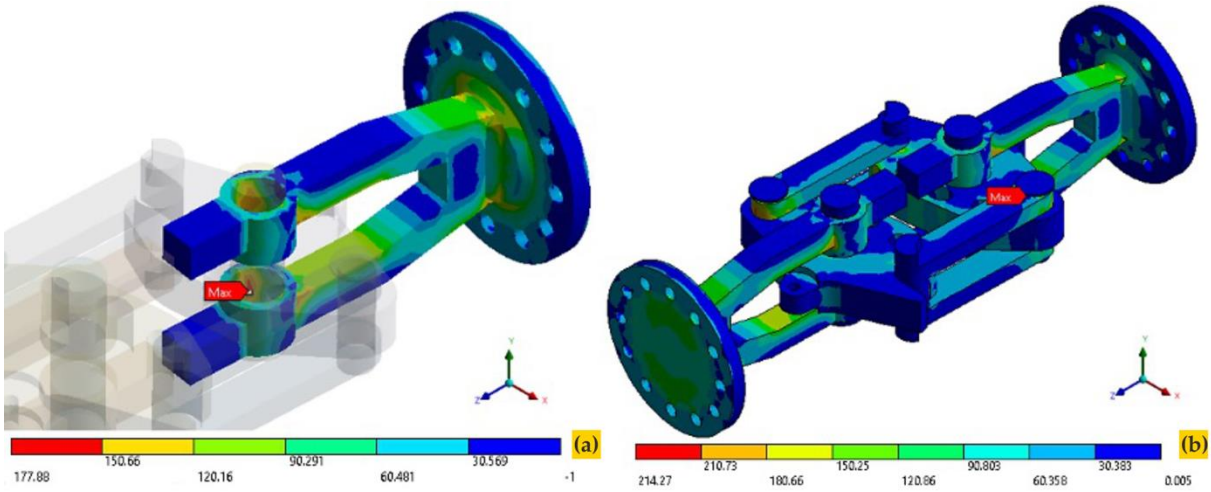

Figure 10. (a) Von Mises stress on body (b) Von Mises stress on assembly

with a factor of safety of 1.12 when compared to the yield stress of the material, as shown in **Figure 10b**. It is important to note that the coupling link component is not included within the scope of the optimization process. Numerical and experimental comparisons were conducted at five critical points and assessed using principal strains, as depicted in **Figure 11**. The strain gauge is strategically positioned at the node with the highest stress in the normal force direction.

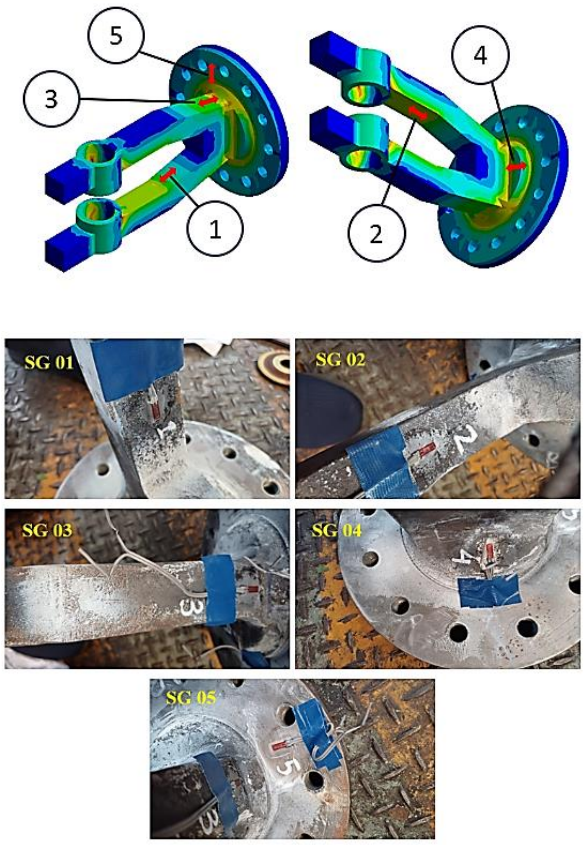

Figure 11. Strain observation points

3.3. *Result of the Prototype Tensile Test*

The tensile testing setup on the RHZ tensile testing machine is depicted in **Figure 12**. The tensile load is applied at a constant speed until it reaches the maximum force or until the specimen is damaged (broken), with data recorded every 2 seconds on the data logger. According to the tensile testing results, the maximum tensile load on the entire automatic coupler assembly is 314 kN, equivalent to 32.02 tons, with a displacement of 21 mm, as illustrated in the graph showing the relationship between the tensile load and machine stroke in **Figure 13**. The failure occurred at the pinhole of the coupling link when the test reached the maximum load.

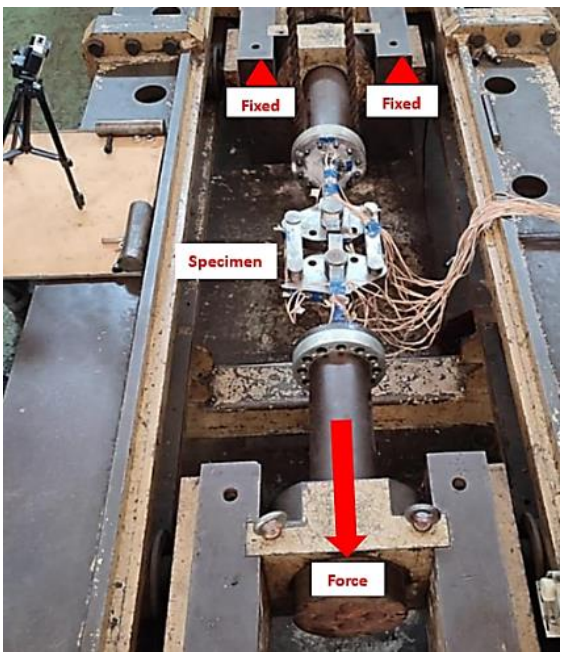

Figure 12. Experimental setup and configuration of the prototype tensile test

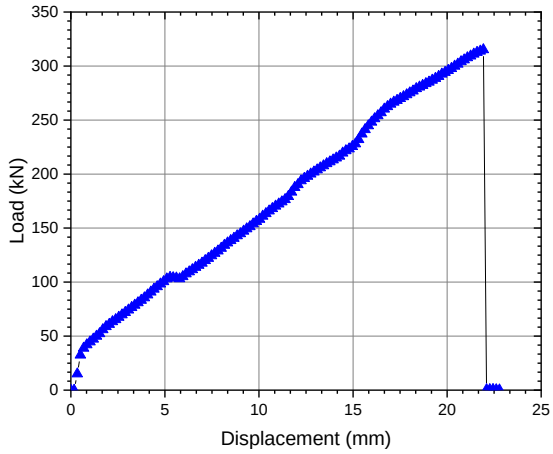

Figure 13. Tensile load vs. displacement graph

3.4. *Numerical and Experimental Comparison*

The validation process undertaken in this study was comprehensive, involving a comparison of the numerical results with experimental data collected from designated strain gauge locations. The experimental data, acquired at each observation point, were precisely logged using data loggers, while the numerical data were generated based on the principal elastic strains computed by the ANSYS solvers. Analysing the five designated observation points depicted in **Figure 14**, it was evident that strain occurred within the elastic region of the material when subjected to a load of 296.65 kN. Point 3 emerged as the location with the highest observed strain, whereas point 5 exhibited the lowest strain among the selected points. The disparities observed at points 1-5 were quantified, revealing errors of 10%, 19%, 5%, 4%, and 6%, respectively.

Figure 15 shows the stress ratios at the five observation points under both a tensile load of 296.65 kN and a maximum tensile load of 314 kN. A comparison between the numerical and experimental results consistently revealed a clear trend: node 3 experiences the highest strain, while node 5 demonstrates the lowest strain. Quantifying these disparities, the errors observed at five points under a tensile load of 296.65 kN were 7%, 15%, 3%, 5%, and 4%. Furthermore, the errors observed at the five points corresponding to the maximum tensile load of 314 kN were 9%, 15%, 3%, 4%, and 11%, respectively. Importantly, with a material yield value of 241 MPa, all five critical points are declared safe, as they only undergo elastic deformation. This thorough comparison establishes the reliability and accuracy of our numerical models under various loading conditions, reinforcing the credibility of our study's findings.

4. Conclusions

- Generative design, in the form of topology optimization, has proven to be effective in reducing the body design mass by 14.42 kg, approximately 46.41%, compared to the mass of the body of the initial model automatic coupler.

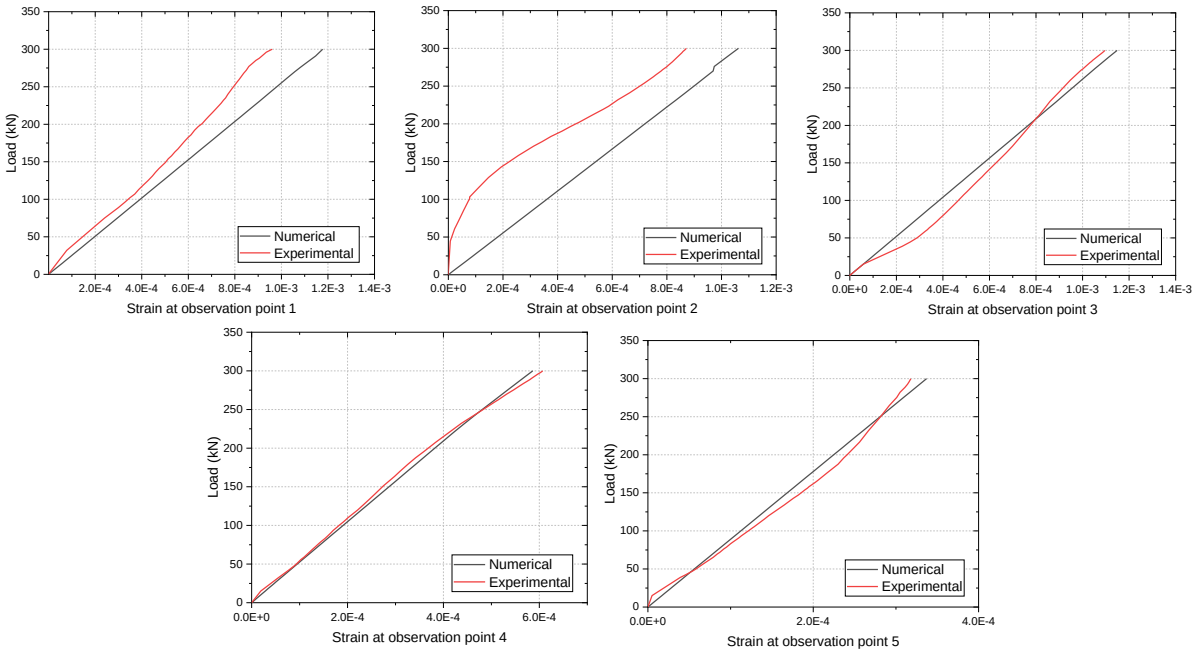

Figure 14. Load vs. strain comparison at 5 observation points

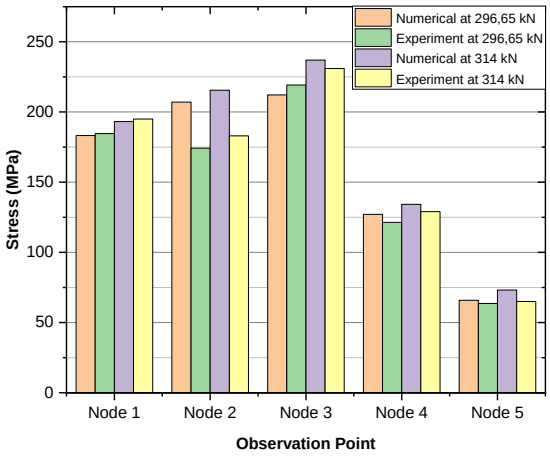

Figure 15. Stress comparison at 5 observation points

- Both the SIMP and the LSM exhibit fairly similar geometric shapes. SIMP demonstrates the advantage of requiring fewer iterations, while LSM provides smoother contour results, facilitating redesign efforts.
- The tensile strength evaluation results indicate that the automatic coupler body, optimized through topology optimization, can withstand a main load of 295.65 kN and a maximum load of 314 kN. Numerical and experimental observations at five points show elastic deformation, which remains below the material yield of 241 MPa.
- This research contributes to the advancement of the next generation of automatic coupler designs, emphasizing key aspects of lightweight design and structural performance.
- The factor of safety in the design is still close to 1, indicating that improvements are needed, one of which could be the use of materials with better mechanical properties. Additionally, there is potential for future research, particularly in evaluating numerical and experimental results on components that experience fractures under maximum load conditions.

Acknowledgments

The authors gratefully acknowledge the financial support provided by the Directorate of Research and Community Service Institut Teknologi Sepuluh Nopember, Indonesia and National Research and Innovation Agency, Indonesia.

Author's Declaration

Authors' contributions and responsibilities

J.M.V.: research design, data analysis, writing original draft, and editing. A.S.P.: conceptualization, funding acquisition, data analysis, reviewing. A.S.: conceptualization, methodology, data analysis and reviewing. L.S.:writing assistance. M.P.: data analysis. K.S.: data analysis, reviewing.

Funding

This research is funded by Directorate of Research and Community Service Institut Teknologi Sepuluh Nopember, Indonesia, with funding agreement letter number 2434/PKS/ITS/2023.

Availability of data and materials

All data are available from the authors.

Competing interests

The authors declare no competing interest.

Additional information

No additional information from the authors.

References

[1] Y. Lei, "Lightweight Design of High-speed Train under the Development of New Materials," in *5th International Conference on Vehicle, Mechanical and Electrical Engineering*, 2020, pp. 217–221, doi: 10.5220/0008865102170221.

[2] E. de la Guerra, "Lightweight primary structures for High-speed railway carbodies," *International Congress on High-speed Rail: Technologies and Long Term Impacts*, vol. 5, pp. 1-9–21, 2018.

[3] D. W. Karmiadji, B. Haryanto, O. Ivano, M. Perkasa, and A. R. Farid, "Bogie Frame Structure Evaluation for Light-Rail Transit (LRT) Train: A Static Testing," *Automotive Experiences*, vol. 4, no. 1, pp. 36–43, 2021, doi: 10.31603/ae.4252.

[4] D. W. Karmiadji, M. Gozali, A. Anwar, H. Purnomo, M. Setiyo, and R. Junid, "Evaluation of Operational Loading of the Light-Rail Transit (LRT) in Capital Region, Indonesia," *Automotive Experiences*, vol. 3, no. 3, pp. 104–114, 2020, doi: 10.31603/ae.v3i3.3882.

[5] A. Cascino, E. Meli, and A. Rindi, "A strategy for lightweight designing of a railway vehicle car body including composite material and dynamic structural optimization," *Railway*

Engineering Science, vol. 31, no. 4, pp. 340–350, Dec. 2023, doi: 10.1007/s40534-023-00312-6.

[6] M. Seitzberger, R. Nedelik, A. Ruthmeier, and T. Grausgruber, "CAE-based concept development for lightweight design of railway vehicles," *Lightweight Design worldwide*, vol. 10, no. 5, pp. 32–37, Oct. 2017, doi: 10.1007/s41777-017-0044-y.

[7] M. Watson, M. Leary, and M. Brandt, "Generative design of truss systems by the integration of topology and shape optimisation," *The International Journal of Advanced Manufacturing Technology*, vol. 118, no. 3–4, pp. 1165–1182, Jan. 2022, doi: 10.1007/s00170-021-07943-1.

[8] H. Sun and L. Ma, "Generative Design by Using Exploration Approaches of Reinforcement Learning in Density-Based Structural Topology Optimization," *Designs*, vol. 4, no. 2, p. 10, May 2020, doi: 10.3390/designs4020010.

[9] S. Jang, S. Yoo, and N. Kang, "Generative Design by Reinforcement Learning: Enhancing the Diversity of Topology Optimization Designs," *Computer-Aided Design*, vol. 146, p. 103225, May 2022, doi: 10.1016/j.cad.2022.103225.

[10] S. Johnsen, "Structural Topology Optimization: Basic Theory, Methods and Applications," Norwegian University of Science and Technology, 2013.

[11] J. Gao, M. Xiao, Y. Zhang, and L. Gao, "A Comprehensive Review of Isogeometric Topology Optimization: Methods, Applications and Prospects," *Chinese Journal of Mechanical Engineering*, vol. 33, no. 1, p. 87, Dec. 2020, doi: 10.1186/s10033-020-00503-w.

[12] P. W. Christensen and A. Klarbring, *An Introduction to Structural Optimization*. Springer, 2008.

[13] P. K. Srivastava, "Reducing Weight of Freight Bogie Bolster Using Topology Optimization," *Revista Gestão Inovação e Tecnologias*, vol. 11, no. 3, pp. 324–339, Jun. 2021, doi: 10.47059/revistageintec.v11i3.1941.

[14] T. Ide, M. Otomori, J. P. Leiva, and B. C. Watson, "Structural optimization methods and techniques to design light and efficient automatic transmission of vehicles with low radiated noise," *Structural and Multidisciplinary Optimization*, vol. 50, no. 6, pp. 1137–1150, Dec. 2014, doi: 10.1007/s00158-014-1143-6.

[15] E. Tyflopoulos, M. Lien, and M. Steinert, "Optimization of Brake Calipers Using Topology Optimization for Additive Manufacturing," *Applied Sciences*, vol. 11, no. 4, p. 1437, Feb. 2021, doi: 10.3390/app11041437.

[16] M. Mrzygłód and T. Kuczek, "Uniform crashworthiness optimization of car body for high-speed trains," *Structural and Multidisciplinary Optimization*, vol. 49, no. 2, pp. 327–336, Feb. 2014, doi: 10.1007/s00158-013-0972-z.

[17] N. M. Patel, B.-S. Kang, J. E. Renaud, and A. Tovar, "Crashworthiness Design Using Topology Optimization," *Journal of Mechanical Design*, vol. 131, no. 6, Jun. 2009, doi: 10.1115/1.3116256.

[18] J. M. Valentino, A. S. Pramono, and A. Syaifudin, "Design Optimization of Hooked Plate on the Automatic Coupler for High-Speed Train," in *Recent Advances in Mechanical Engineering*, 2023, pp. 10–18.

[19] ASME, "Guide for Verification and Validation in Computational Solid Mechanics," *American Society of Mechanical Engineers*, no. March, pp. 1–53, 2006.

[20] J. Mario, A. Syaifudin, A. S. Pramono, A. Windharto, and A. Farid, "Synthesis Analysis to Improve Coupling Strength of Automatic Coupler," Mar. 2023, pp. 67–73, doi: 10.4028/p-higyh1.

[21] M. P. Bendsøe and O. Sigmund, *Topology Optimization: Theory, Methods, and Applications*. Berlin, Heidelberg: Springer Berlin Heidelberg, 2004.

[22] M. Abdi, "Evolutionary topology optimization of continuum structures using X-FEM and isovalues of structural performance," University of Nottingham, 2015.

[23] P. Wei, W. Wang, Y. Yang, and M. Y. Wang, "Level set band method: A combination of density-based and level set methods for the topology optimization of continuums," *Frontiers of Mechanical Engineering*, vol. 15, no.

3, pp. 390–405, Sep. 2020, doi: 10.1007/s11465-020-0588-0.

[24] W. Zuo and K. Saitou, "Multi-material topology optimization using ordered SIMP interpolation," *Structural and Multidisciplinary Optimization*, vol. 55, no. 2, pp. 477–491, Feb. 2017, doi: 10.1007/s00158-016-1513-3.

[25] R. Picelli, S. Townsend, C. Brampton, J. Norato, and H. A. Kim, "Stress-based shape and topology optimization with the level set method," *Computer Methods in Applied Mechanics and Engineering*, vol. 329, pp. 1–23, Feb. 2018, doi: 10.1016/j.cma.2017.09.001.

[26] S. Liu, Q. Li, J. Liu, W. Chen, and Y. Zhang, "A Realization Method for Transforming a Topology Optimization Design into Additive Manufacturing Structures," *Engineering*, vol. 4, no. 2, pp. 277–285, Apr. 2018, doi: 10.1016/j.eng.2017.09.002.

[27] M. Noda, K. Matsushima, and T. Yamada, "Orientation optimization via topological derivatives in combination with multi-material topology optimization based on extended level set method," *Computer Methods in Applied Mechanics and Engineering*, vol. 418, p. 116585, Jan. 2024, doi: 10.1016/j.cma.2023.116585.

[28] ASTM, "Standard test methods for tension testing of metallic materials E8/E8M," 2013. doi: 10.1520/E0008.

[29] J. Valentino *et al.*, "Enhancing S45C steel for the primary component of an automatic coupler using quench-tempering techniques," *Journal of Applied Engineering Science*, vol. 22, no. 2, pp. 215–222, 2024, doi: 10.5937/jaes0-43988.

[30] P. Arasaratnam, K. S. Sivakumaran, and M. J. Tait, "True Stress-True Strain Models for Structural Steel Elements," *ISRN Civil Engineering*, vol. 2011, pp. 1–11, Aug. 2011, doi: 10.5402/2011/656401.

[31] M. Jeyakumar and T. Christopher, "Influence of residual stresses on failure pressure of cylindrical pressure vessels," *Chinese Journal of Aeronautics*, vol. 26, no. 6, pp. 1415–1421, Dec. 2013, doi: 10.1016/j.cja.2013.07.025.

[32] Y. L. Yap *et al.*, "Topology optimization and 3D printing of micro-drone: Numerical design with experimental testing," *International Journal of Mechanical Sciences*, vol. 237, p. 107771, Jan. 2023, doi: 10.1016/j.ijmecsci.2022.107771.

[33] B. Xie, X. Wu, L. Liu, and Y. Zhang, "Topological Design of a Hinger Bracket Based on Additive Manufacturing," *Materials*, vol. 16, no. 11, p. 4061, May 2023, doi: 10.3390/ma16114061.

[34] P. K. Sahoo, S. Pattnaik, and M. K. Sutar, "A State-of-the-Art Review on Manufacturing and Additive Influences on Sand-Cast Components," *Arabian Journal for Science and Engineering*, vol. 44, no. 12, pp. 9805–9835, Dec. 2019, doi: 10.1007/s13369-019-04139-4.

[35] M. Maass, W. A. Deutsch, and F. Bartholomai, "Magnetic Particle Inspection on train components," 2014.

[36] M. Gupta, M. A. Khan, R. Butola, and R. M. Singari, "Advances in applications of Non-Destructive Testing (NDT): A review," *Advances in Materials and Processing Technologies*, vol. 8, no. 2, pp. 2286–2307, Apr. 2022, doi: 10.1080/2374068X.2021.1909332.

[37] P. Tutak, "Application Of Strain Gauges In Measurements Of Strain Distribution In Complex Objects," *Journal of Applied Computer Science Methods*, vol. 6, no. 2, pp. 135–145, Dec. 2014, doi: 10.1515/jacsm-2015-0004.

[38] J. Arpin-Pont, M. Gagnon, A. S. Tahan, A. Coutu, and D. Thibault, "Methodology for estimating strain gauge measurement biases and uncertainties on isotropic materials," *The Journal of Strain Analysis for Engineering Design*, vol. 50, no. 1, pp. 40–50, Jan. 2015, doi: 10.1177/0309324714550116.